



Aalborg Universitet

AALBORG UNIVERSITY
DENMARK

Reliability-Driven Assessment of GaN HEMTs and Si IGBTs in 3L-ANPC PV Inverters

Gurpinar, Emre; Yang, Yongheng; Iannuzzo, Francesco; Castellazzi, Alberto; Blaabjerg, Frede

Published in:

I E E E Journal of Emerging and Selected Topics in Power Electronics

DOI (link to publication from Publisher):

[10.1109/JESTPE.2016.2566259](https://doi.org/10.1109/JESTPE.2016.2566259)

Publication date:

2016

Document Version

Accepted author manuscript, peer reviewed version

[Link to publication from Aalborg University](#)

Citation for published version (APA):

Gurpinar, E., Yang, Y., Iannuzzo, F., Castellazzi, A., & Blaabjerg, F. (2016). Reliability-Driven Assessment of GaN HEMTs and Si IGBTs in 3L-ANPC PV Inverters. *I E E E Journal of Emerging and Selected Topics in Power Electronics*, 4(3), 956-969. <https://doi.org/10.1109/JESTPE.2016.2566259>

General rights

Copyright and moral rights for the publications made accessible in the public portal are retained by the authors and/or other copyright owners and it is a condition of accessing publications that users recognise and abide by the legal requirements associated with these rights.

- Users may download and print one copy of any publication from the public portal for the purpose of private study or research.
- You may not further distribute the material or use it for any profit-making activity or commercial gain
- You may freely distribute the URL identifying the publication in the public portal -

Take down policy

If you believe that this document breaches copyright please contact us at vbn@aub.aau.dk providing details, and we will remove access to the work immediately and investigate your claim.

Reliability-Driven Assessment of GaN HEMTs and Si IGBTs in 3L-ANPC PV Inverters

Emre Gurpinar, *Student Member, IEEE*, Yongheng Yang, *Member, IEEE*,
Francesco Iannuzzo, *Senior Member, IEEE*, Alberto Castellazzi, *Fellow, IEEE*

Abstract—In this paper, thermal loading of the state-of-the-art GaN HEMTs and traditional Si IGBTs in 3L-ANPC PV inverters is presented considering real-field long-term mission profiles (i.e., ambient temperature and solar irradiance). A comparison of Si IGBT against GaN HEMT with three different possibilities: 1) with TIM at 10 kHz, 2) without TIM at 10 kHz, and 3) with TIM at 300 kHz has been performed. The assessment results indicate lower thermal stress with GaN HEMT devices at 10 kHz in comparison to Si IGBT. At high switching frequencies, the results show significant system level cost savings can be achieved without compromise of operating efficiency with GaN HEMTs. Both simulations and experimental tests are provided to demonstrate the thermal loading analysis approach. More important, the proposed analysis and comparison approach can be used for lifetime and reliability analysis of wide-bandgap devices.

Index Terms—Wide bandgap (WBG) power devices, gallium-nitride (GaN), thermal loading analysis, reliability, three-level active neutral point clamped (3L-ANPC) converter, photovoltaic (PV) systems

I. INTRODUCTION

RENEWABLE power generation is one of the main focus areas of highly efficient power electronic systems due to the increasing demand for clean power resources. Photovoltaic (PV) energy is a key renewable energy resource along with hydro and wind, and as of 2013, the global installed PV capacity has been over 138 GW with a potential of 160 TWh energy generation every year. In addition to the current-installed capacity, the worst case scenario for annual PV installation until 2018 is expected to be around 35 GW [1]. Even with the worst case scenario, there is a strong demand for energy generation with PV systems, where power electronic converters are vital components for realisation of this demand. Basically, the power electronic converters provide two main tasks for PV systems: 1) maximisation of energy utilisation by means of Maximum Power Point Tracking (MPPT) control; 2) integration with an AC grid by converting the generated electricity from DC to AC (i.e., using DC-AC inverters) in a grid-friendly manner. That is to say, a certain amount of demands to PV systems should be taken into account in the planning, design, and operation phases. For instance, different converter topologies and system structures based on

single- and double-staged conversion systems are published and reviewed in literature [2]–[4], whereas aforementioned power electronics converters are widely utilized.

For maximisation of energy generation and minimisation of system payback time, efficiency of power electronic converters in PV applications is always one of the key parameters along with reliability and lifetime in those applications. Therefore, efficiency improvement of power electronic systems has been an important aspect of research in renewable energy. Transformerless inverter topologies have been proposed that introduce additional power switches for maintaining high efficiency while minimizing the leakage ground current without presence of the galvanic isolation between PV panels and the grid [5], [6]. Along with new transformerless topologies, emerging wide-bandgap (WBG) devices such as SiC Schottky diodes, SiC JFETs, SiC MOSFETs and GaN HEMTs have been introduced to PV converters due to superior properties of WBG materials [7]. Application of WBG devices in DC/DC converters and DC/AC inverters for PV systems has been widely discussed in the literature. Various converters with different application conditions show the potential of achieving very high efficiencies with WBG devices under a wide operating range.

For example, the performance of SiC JFET devices for PV applications has been discussed in details in [8]–[10]. A number of experimental test results show a peak efficiency of 98.8% and in [8], the Highly Efficient and Reliable Inverter Concept (HERIC) converter with SiC devices has achieved a 99% peak efficiency. As demonstrated in [9], the overall losses in a PV inverter can be halved by just replacing conventional Si IGBTs with SiC JFETs, and thus efficiency can be improved. Although SiC JFETs had promising results, the gate drive complexity and normally-on characteristic of the devices were the main obstacles for applications in commercial products [11]. Alternatively, SiC MOSFETs have been introduced at 600 V and 1200 V blocking class range for renewable applications from different manufacturers, and the performances of these devices in various topologies are discussed in [12X][14X] [12]–[14]. Similar to the results with SiC JFETs, replacing Si IGBTs with SiC MOSFETs can bring up to 1% efficiency gain for the same switching frequency. In [13], the performance of SiC MOSFETs and Si IGBTs at 600 V class has been presented, where it shows that the SiC MOSFETs under different ambient temperatures can operate without malfunctions. In addition, all SiC-based 3-level T-type inverters can achieve peak efficiency 98.3% at 16 kHz switching frequency.

E. Gurpinar and A. Castellazzi are with the Power Electronics, Machines and Control (PEMC) research group, Tower Building, University of Nottingham, University Park, Nottingham, NG7 2RD, U.K. (email: emre.gurpinar@nottingham.ac.uk; alberto.castellazzi@nottingham.ac.uk).

Yongheng Yang, Francesco Iannuzzo and Frede Blaabjerg are with Department of Energy Technology, Aalborg University, 9220 Aalborg, Denmark (email: yoy@et.aau.dk; fia@et.aau.dk; fbl@et.aau.dk).

Recent findings show that the WBG power devices suitable for grid connected applications are normally-off GaN HEMTs at a blocking class of 600 V. Such GaN normally-off HEMTs have been introduced by Panasonic at 600 V and GaN Systems at 650 V. There are several practical applications with those WBG devices. For instance, in [15], GaN HEMTs are implemented in a DC/DC converter for the MPPT control in PV applications, and the converter operated with a peak efficiency of 98.59% at 48 kHz switching frequency. Furthermore, the same devices have been used in other applications such as resonant LLC DC/DC converters, three phase inverters and synchronous buck converters. Those cases have shown the high switching and conduction performance of the GaN HEMT devices in different operating conditions [16]–[20]. Specifically, in [17], GaN devices are demonstrated on a three phase inverter with 99.3% efficiency at 900 W output power and 16 kHz switching frequency. Finally, GaN HEMTs are demonstrated along with 1200 V SiC MOSFETs in single-phase PV applications in [19], [20], where the converter has achieved 99.2% peak efficiency at 1.4 kW output power and 16 kHz switching frequency. The presented converter proves the stable operation of WBG devices under wide load, switching frequency and ambient temperature conditions. Furthermore, normally-on GaN HEMTs at 600 V voltage class with and without cascode structures are discussed in [21] and [22] for hard-switching topologies. Performance improvement in a synchronous buck topology is presented in [20X] and it is shown that smaller reverse recovery charge and output capacitance of GaN HEMTs lead to reduction in turn-on losses and up to 2% efficiency improvement in comparison to Si MOSFET. The current collapse phenomena for 600 V normally-on GaN HEMT is presented in [22]. Although the device is statically rated at 600 V, the experimental results are presented up to 50–60 V due to increase in on-state voltage drop during dynamic testing. Nevertheless, the above literature survey shows that WBG based power converters can deliver very high efficiency at switching frequencies that is not possible with conventional Si-based power devices.

In addition to high efficiency, high reliability is required for PV inverters in order to extend lifetime of the system and therefore energy generation [23], and as a consequence to reduce the cost of energy. Commercial PV inverters are generally offered with a 25 year performance warranty, and also considered as the most vulnerable components in a PV system [24]. It is known from field data that a majority of the failure mechanisms for PV inverters are related to mean temperature variations and temperature swings [25]; therefore long-term mission-profile plays a key role in reliability and assessment of thermal performance of the inverter [26], [27]. During design process, real-field operating conditions (e.g., ambient temperature and solar irradiance) have to be considered for reliability-oriented approaches, as different conditions may unevenly stress the components within the system. Emerging SiC and GaN power devices have different electrical and thermal properties from Si devices due to inherent differences in material, chip size and packaging properties [28]. Therefore, it is essential to evaluate the long-term performance of the system for better understanding the benefits as well as the

drawbacks of using WBG devices in PV systems. In such a way, the applications of WBG devices can further be paved away.

In this paper, a reliability-oriented comparison of conventional Si IGBTs with state-of-the-art GaN HEMTs for 3L-ANPC PV systems is thus presented. In Section II, converter topology, modulation strategy and power device properties are presented, followed by a mission-profile oriented analysis in terms of thermal loading and reliability estimation of the considered power electronic converters. Simulation results of the converter based on GaN and Si devices are presented in Section III regarding efficiency, annual energy generation, loss distribution and thermal loading. Finally, experimental results of the GaN-based prototype (i.e., 3L-ANPC inverter) at different load conditions are presented before the conclusion.

II. 3L-ANPC INVERTER AND PV SYSTEM

A. ANPC Topology and Modulation Scheme

Active neutral point clamped (ANPC) inverter is a member of half-bridge neutral point clamped inverter family and it was introduced in [29] as an alternative to neutral point clamped (NPC) inverter [30] for improved loss balancing and better utilization of semiconductor chip areas in the inverter. Replacing diodes in NPC inverters with active switches provides additional zero states, and at the same time different modulation strategies can be applied with a flexible utilization of the redundant switching states. The topology has been discussed thoroughly for industrial drive applications in literature [31]–[33]. The schematic of the studied converter for a double-stage three-phase grid-connected PV system is presented in Fig. 1. As it can be observed, each leg of the 3L-ANPC inverter is formed by 6 active switches (S_1 – S_{18} of three legs) in order to achieve a three-level phase output voltage with respect to the neutral point N, and the power devices (S_1 – S_{18}) are rated at half of the DC link voltage V_{DC} . Consequently, it is possible to use GaN HEMT devices at 600 V class for three-phase grid-connected applications, where the DC link voltage is within a range of 650–1000 V. In this configuration, a DC-DC converter between the PV strings and the 3L-ANPC inverter is adopted in order to flexibly maximize the energy production (i.e., MPPT control) as well as to extend the operating hours of the PV systems (e.g., in the case of weak solar irradiance). The power delivered by the DC/DC converter is then fed to the 3L-ANPC inverter, while the DC-link voltage is usually maintained as constant by controlling the inverter. Normally, for the PV system, it should inject high-quality grid currents at unity power factor operation, and thus the modulation schemes applied to the 3L-ANPC inverter should be specially designed.

Different modulation strategies can be implemented for the 3L-ANPC inverter in order to achieve a balanced switching loss distribution or doubling of the effective switching frequency at the output [34]. Solutions proposed in [31]–[33], [35] are limited to the use of Si devices and were optimised for IGBTs as well as for MOSFETs. A modulation strategy based on reverse conduction capability of SiC MOSFETs has been introduced in [12] for a single-phase leg, as further shown in Fig. 2. It can be seen from the driving signals that there are

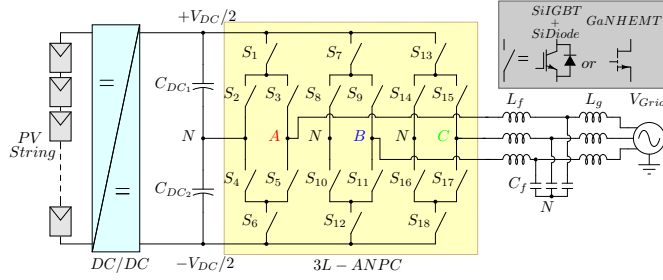


Fig. 1: Grid-connected three-phase double-stage 3L-ANPC inverter with an LCL filter in PV applications

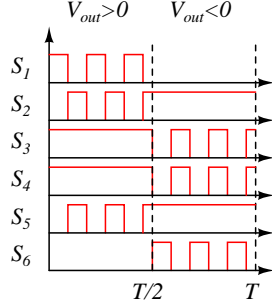


Fig. 2: Switching sequences for leg-A of the 3L-ANPC inverter [12].

four operating states: 1) positive voltage, 2) zero state positive current, 3) zero state negative current and 4) negative voltage. Specifically, taking leg-A shown in Fig. 1 as an example, the positive voltage is applied to the output of the phase leg by turning-on S_1 and S_3 and the output current flows through the two devices in series. During the positive active-state, S_4 ensures an equal DC link voltage sharing between S_5 and S_6 without conducting any current. The transition from positive active-state to zero-state is accomplished by switching S_1 off, and then simultaneously switching S_2 and S_5 on, and thus the current is divided in two parallel paths: $S_2 - S_3$ and $S_4 - S_5$. Same commutation scheme is used for complementary switches during the negative active-state and the zero-state. This modulation method ensures low conduction losses at zero-states, and the outer switches (S_1 and S_6) are exposed to switching losses at unity power factor. In a Si-based converter, IGBTs with antiparallel diodes can be employed; while in GaN based converter, only HEMTs will be sufficient because of the reverse conduction capability of HEMT devices. Therefore, although the number of active devices in Si and GaN will be the same, the number of total switches will be half in GaN based inverter due to the absence of antiparallel diodes, leading to reduced converter volume as well as heatsink size.

B. System and 3L-ANPC Parameters

The PV system and converter parameters considered in this study are presented in Table I. As the DC/DC converter between PV strings and the 3L-ANPC inverter that is shown in Fig. 1 is responsible from the MPPT control, it is assumed that the conversion efficiency of 99% can be achieved by the MPPT control of the converter in the following. Recent

TABLE I: Converter and System Parameters

Parameter	Value
Input DC Link Voltage (V_{DC})	800 V
Input Power (P_{in}) @ 25 °C, 1000 W/m ²	6 kW
Switching Frequency (f_{sw})	10 kHz - 300 kHz
DC Link Capacitor ($C_{DC1} - C_{DC2}$)	1500 μ F
Output Filter Inductor (L_f)	3.6 mH
Output Filter Capacitor (C_f)	2.35 μ F
Output Filter Capacitor (L_g)	4 mH
Grid Phase-to-Phase Voltage (V_{ph-ph})	400 Vrms
PV Module	BP 365
PV String Configuration	46 module each - 2 strings
DC/DC (MPPT) Efficiency (η_{MPPT})	99 %

advances in SiC MOSFETs show that efficiency higher than 99% is feasible for DC/DC converters in PV applications [36]. Two parallel-connected PV strings, formed by 46 PV modules, are considered to deliver 6 kW power at the standard test conditions (i.e., 25 °C ambient temperature and 1000 W/m² solar irradiance). The input power P_{in} can go up to 11 kW at -25 °C and 1500 W/m² theoretically, and therefore the total rating of the converter is selected as 15 kW in order to operate at a wide range of ambient temperature and solar irradiance. The inverter is operated at 10 kHz switching frequency for Si IGBTs; while at 10 kHz and 300 kHz for GaN HEMT devices for evaluation of the performance of GaN HEMT based inverter at low and high switching frequencies in comparison to the Si IGBT based inverter. Selection of 300 kHz for high frequency application of the GaN HEMTs is determined by the operation point of the converter, where the junction temperature of most stressed devices is close to their limits, and the efficiency is still higher than the Si IGBT based converter. Additionally, it is shown in [37] that by moving 10 kHz to 300 kHz, 70 % reduction in EMC filter volume can be achieved for GaN HEMTs.

C. 650V GaN HEMT and 600V Si IGBT

As previously discussed, the GaN HEMT devices have superior switching properties in comparison to Si IGBTs or Si MOSFETs. At the 600 V blocking class, super-junction (SJ) Si MOSFETs can be an alternative to WBG devices, where a unipolar current conduction must be employed due to the poor body-diode characteristic of SJ devices [38], [39]. Since the 3L-ANPC inverter requires bipolar current condition; the comparison is limited to IGBT in Si-based devices in this study. Device properties of the selected GaN HEMT and Si IGBT are presented in Table II. Both devices are at the 600 V blocking class and suitable for full bridge topologies with 400 V DC link or multi-level topologies with 800 V DC link with the grid voltage of 230 Vrms. As it can be seen in Table 2, the Si IGBT continuous current rating is almost equal to rating of GaN HEMT device at 100 °C, and therefore a fair comparison can be conducted between the two device technologies. Si IGBT switching losses are expected to be higher than GaN HEMTs. Regarding on-state losses, the GaN HEMT has better conduction performance in comparison to Si

TABLE II: Converter and System Parameters

	GaN Systems GaN E-HEMT GS66508T	Infineon Si IGBT IKP20N60H3
Drain-Source Voltage (V_{DS})	650 V	600 V
Continuous Drain Current (I_{DS})	23 A @ 100 °C	20 A @ 100 °C
Drain-Source On-State Resistance ($R_{DS(on)}$)	55 mΩ @ 25 °C 129 mΩ @ 100 °C	N/A
Collector-Emitter Saturation Voltage ($V_{CE(sat)}$)	N/A	1.95 V @ 25 °C 2.5 V @ 100 °C
Input Capacitance (C_{iss})	200 pF	1100 pF
Output Capacitance (C_{oss})	67 pF	70 pF
Reverse Transfer (C_{rss})	2 pF	32 pF
Gate Charge (Q_g)	6.5 nC	120 nC
Min. Gate Threshold Voltage (V_{th})	1.6 V	4.1 V
Maximum Junction Temperature (T_j)	150 °C	175 °C
Reverse Recovery Charge (Q_{rr})	0 μC	0.39 μC
Package Stray Inductance (L_σ)	0.4 nH	7 nH
Device Package	GaN _{PX}	TO220-3

IGBT at lower case temperatures. The on-state performances of two technologies are presented in Table II. It can be seen that, the variation of on-state performance of GaN HEMT is more sensitive to junction temperature increase in comparison to Si IGBT. Furthermore, it is shown in Table II that the device capacitance and reverse recovery characteristics of the GaN HEMTs are excellent in comparison to those of the Si IGBTs in the switching dynamics. This switching loss difference has an impact on the device loss distribution, which will be presented in simulations (Section III), as only two devices out of six in the 3L-ANPC leg are subject to switching losses.

In addition to the electrical parameters in Table II, it should be noted that the GaN HEMT device is packaged in a novel structure called GaN_{PX}. The package integrates and encapsulates the GaN HEMT die into a very thin (0.45mm total thickness) high temperature fibreglass matrix. Copper micro vias are used for vertical connections to facilitate heat transfer from top side and electrical connections from the bottom side of the package. The GaNPX technology eliminates bond wires and solders joints, and achieves extremely low stray inductance [40]. As indicated in Table ??, the stray inductance of the GaN HEMT package has 17.5 times less stray inductance per device than that of the Si IGBT package, relying on manufacturer information. This is a key aspect for drawing the maximum benefit from the WBG power devices. Also, by using thick redistribution layer and copper on top of the die, competitive thermal impedance can be ensured.

Nevertheless, the thermal loading of the power electronic devices is still the major lifetime affecting factor, which is an essential part for reliability analysis. Hence, a thermal model of a single device is presented in Fig. 3. The device thermal network consists of thermal impedances between device junction and device case ($Z_{th(jc)}$), case and heat sink ($Z_{th(ch)}$), and heat sink and ambient ($Z_{th(ha)}$). Based on manufacturer datasheets and SPICE models, Foster network parameters for junction-to-case impedance are presented in Table III. Obtained Foster network parameters are transferred to the Cauer network in the simulation environment for accurate thermal modelling. In the case of the GaN device, due its comparatively small dimensions, a satisfactory thermal description was achieved with only one RC group, whereas 3

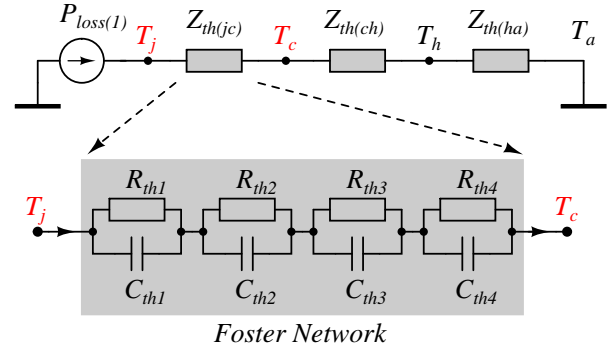


Fig. 3: Thermal model of a single power device, where the RC layer number is related to the device packaging technology as indicated in Table III.

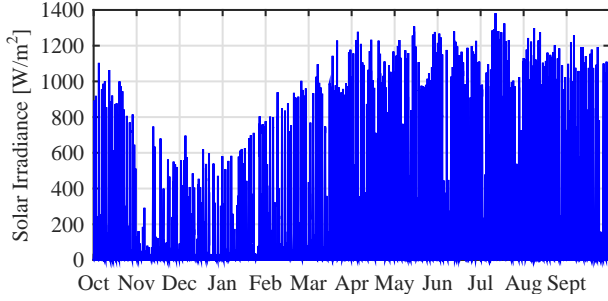
groups have been used for the larger device and package types. Notably, the device thermal model is implemented along with the electrical model (see Fig. 1) in order to obtain the thermal performance with respect to converter instantaneous loading conditions, which are highly dependent on the solar and ambient temperature profiles and in return affect the semiconductor switch properties. One important aspect to consider for GaN HEMTs is the insulation of thermal pad of the device from heat sink where common heat sink is used for the inverter and DC/DC converter. As the thermal pad of GaN HEMTs is directly connected to the substrate and source of the device internally, electrical isolation has to be provided in common heatsink applications. The thermal pad area of GaN HEMT is 20.5 mm² and with a commercial thermally-conductive insulator, which has 3.5 W/m.K thermal conductivity, 0.3 mm thickness and 4 kV breakdown voltage [41]. Thus, an additional thermal resistance of 4 °K/W is added to $Z_{th(ch)}$ in Fig. 3. The additional thermal resistance from the insulator increases the junction temperature of devices significantly due to the thermal pad size even at low switching frequencies. For Si IGBTs, thermally-conductive insulator with 0.57 °K/W thermal resistance and 4 kV breakdown voltage is considered for isolation of discrete devices from common heat sink [42]. The common heat sink for the devices is modelled as a simple RC circuit. There are two reasons for this simplification: 1) The analysis in this study focuses on the thermal profile analysis of steady-state device junction temperature and the heat sink will not have significant effect on thermal loading comparison, 2) Simplification of heat sink model lead to acceleration of long-term mission profile simulations. Junction temperature comparisons with and without insulator will be presented over an annual mission profile by simulations in Section III.

D. Mission-Profile Based Simulation

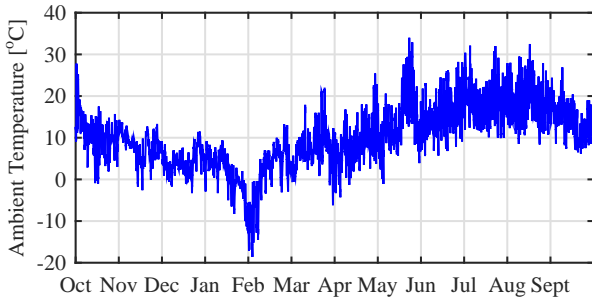
It is necessary to evaluate the performance of power electronic systems in long-term operation along with short-term operation, as the long-term operation profiles can have significant impact on efficiency, reliability and lifetime of the entire system [25]. For short-term evaluation, time-based simulation

TABLE III: Thermal parameters for Si IGBT, Si Diode and GaN HEMT.

Impedance i		$Z_{th(j-c)}$			
		1	2	3	4
Si IGBT	R_{thi} [$^{\circ}\text{K/W}$]	0.07041042	0.3070851	0.3198984	0.1871538
	τ_i [s]	0.000096	0.00068	0.01084623	0.06925485
Si Diode	R_{thi} [$^{\circ}\text{K/W}$]	0.4398	0.6662	0.4734	0.3169
	τ_i [s]	0.00013	0.0011	0.0071	0.04629
GaN HEMT	R_{thi} [$^{\circ}\text{K/W}$]	0.05	-	-	-
	τ_i [s]	0.00025	-	-	-



(a)



(b)

Fig. 4: An annual mission profile used in this paper: (a) solar irradiance and (b) ambient temperature profile in Aalborg.

tools or prototype based experiments can be conducted to assess the performance but both of these approaches are not suitable for long-term evaluation due to constraints of time, computational and financial resources. Therefore an efficient method is required to evaluate the long-term performance (see Figs. 5 and 7) [25], [26]. The long term PV mission profile consists of solar irradiance level (S_i) and ambient temperature (T_a). In this study, a real-field annual PV mission profile data (i.e., solar irradiance level and ambient temperature) in Aalborg is considered. The measured annual solar irradiance and ambient temperature data are presented in Fig. 4.

Realisation of the long-term mission profile based analysis is presented in Fig. 5. The first step of this analysis is to obtain the maximum power (P_m) operation points with respect to the PV module output voltage (v_{pv}) for the PV string specified in Table I, based on the measured different solar irradiance (S_i) and ambient temperature (T_a). Then maximum power and operation voltage is fed into the short-term simulation model in order to obtain power loss (P_{tot}) and temperature profile (T_j) for each switching device in correspondence to

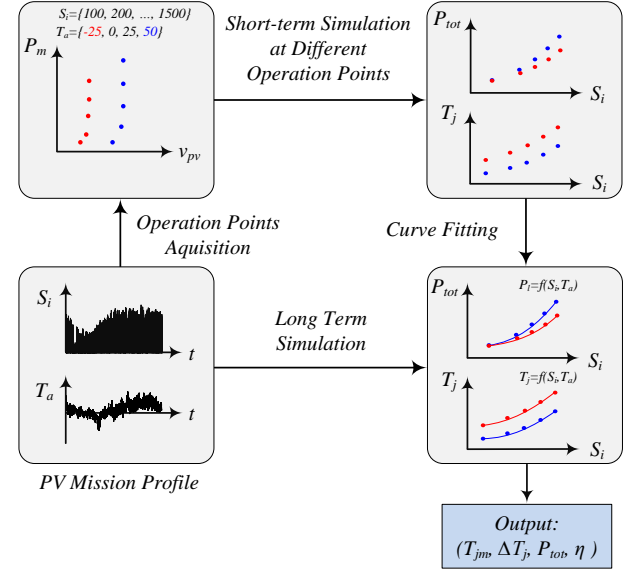


Fig. 5: Realisation of the long-term mission profile based analysis approach.

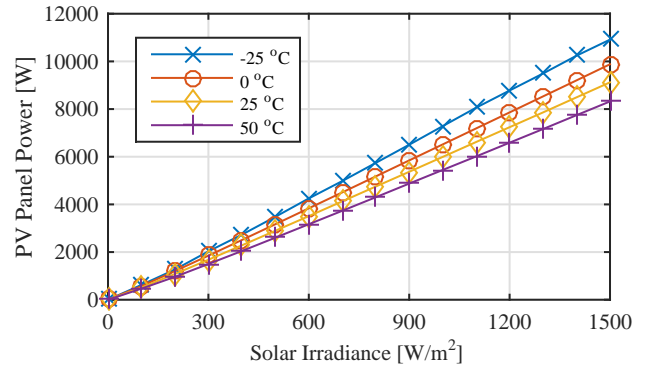


Fig. 6: PV panel output power with respect to solar irradiance and ambient temperature.

an individual operation point (e.g., $P_m = 6$ kW, $V_{pv} = 400$ V for the case of 25°C and 1000 W/m^2). The maximum output power of the PV panel with respect to solar irradiance and ambient temperature is presented in Fig. ???. The losses and temperature performance are finally curve-fitted with respect to the entire solar irradiance and ambient temperature spectrums in such a way to link a specific mission profile with the power electronic converter (electrical behaviour). It should be pointed out here that the MPPT control (dc-dc converter) efficiency has been assumed to 99%, since the focus of this paper is not on the MPPT control.

The detailed structure of the multi-disciplinary analysis method can be seen in Fig. 7. Short-term simulation model consists of two domains: thermal model and electrical model, which are linked via power device model. Electrical parameters affecting conduction and switching losses are fed to the power device model along with junction temperature from the thermal model in order to calculate power device losses with respect to pre-defined switching and conduction performance

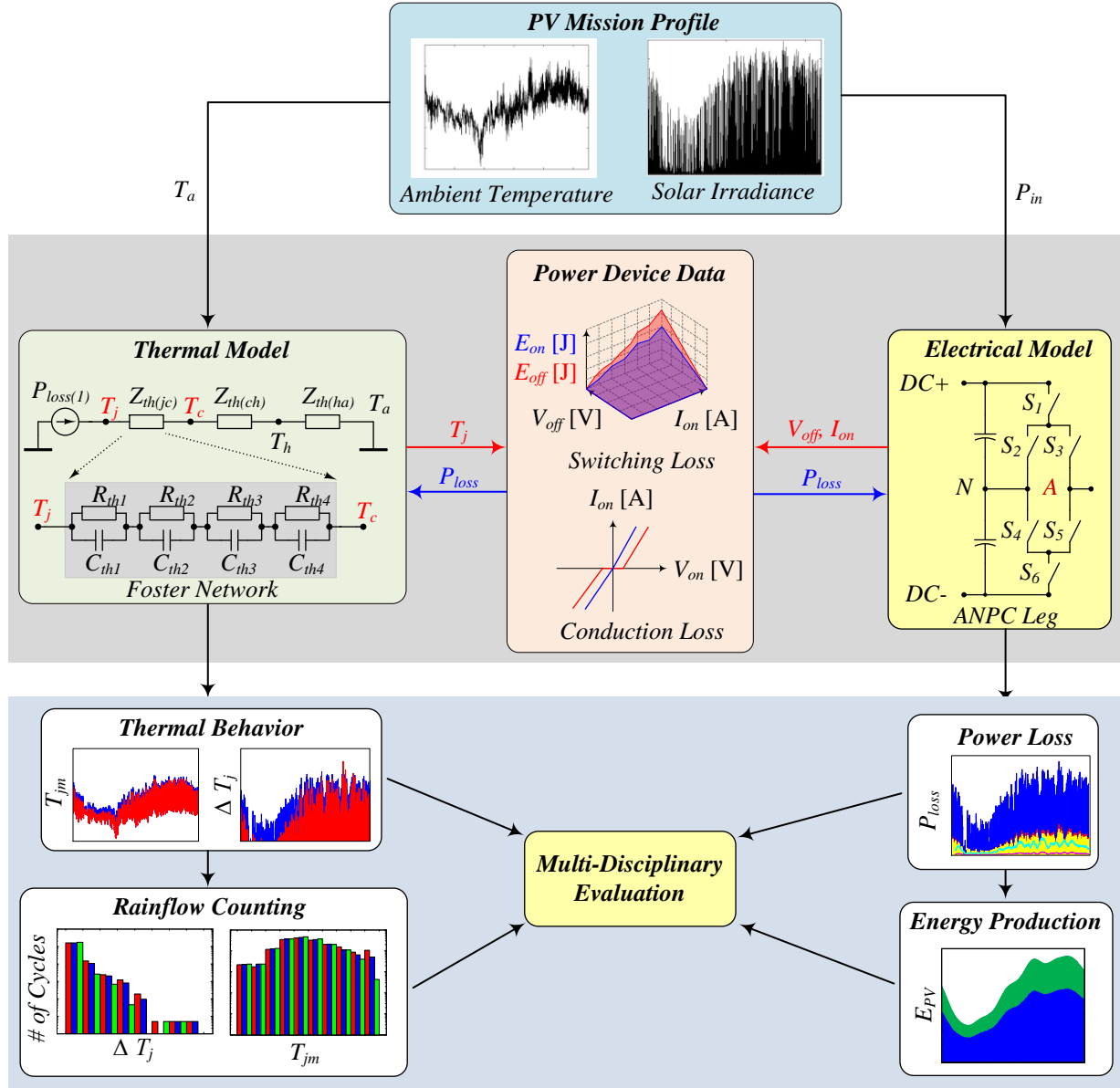


Fig. 7: Multi-disciplinary analysis method.

data. Then, the calculated power loss is fed to thermal model in order to recalculate the junction temperature and to the electrical model for calculation of the total converter losses. This bidirectional data exchange between different simulation domains provide results that can be used for better understanding the thermal and electrical performance, enabling the multi-disciplinary evaluation of the implemented modulation scheme, power devices and converter topologies. Power device data can be obtained from detailed device datasheets that provide switching and conduction loss performance or double pulse tests.

III. SIMULATION RESULTS

The simulations based on the approach explained in details in the previous section are carried out on a single phase 3L-ANPC inverter with the assumption of a balanced three phase grid system and operation. In this case, the analysis

results can be extended to the three-phase 3L ANPC converter shown in Fig. 1. Input power, total conduction losses and total switching losses are recorded for converter performance evaluation according to the multi-disciplinary approach. In addition to this, power losses, mean and maximum junction temperatures for each device are recorded for device in order to evaluate the loss distribution, thermal stress and behaviour of each power switch in a single 3L-ANPC leg. In the beginning of this section, overall inverter performance is presented including inverter loss breakdown, annual power loss and cumulative energy loss for IGBT and GaN based scenarios. These results are followed by the thermal stress comparison of each power device including the power loss distribution, mean junction temperature and junction temperature variation for most stressed devices in the specific configuration.

A. Overall Power Loss and Energy Generation

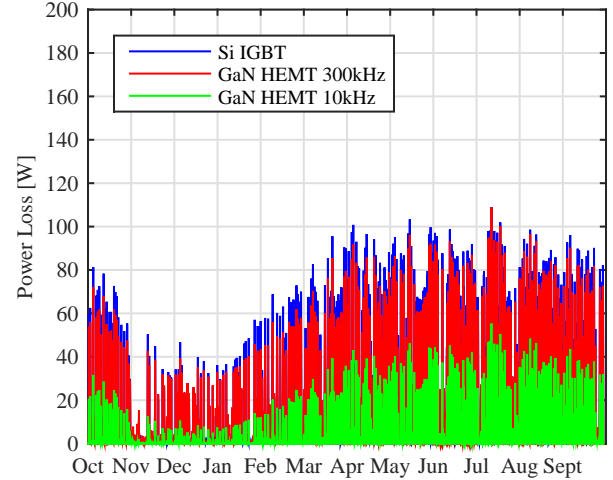
The annual power loss and cumulative energy loss of three-phase 3L-ANPC inverter with Si IGBTs at 10 kHz, and with GaN HEMTs at 10 kHz and 300 kHz are presented in Fig. 8. As it is expected from the results presented in literature, the GaN-based 3L-ANPC inverter has a higher efficiency, and therefore less power losses throughout the year in comparison to those of the Si IGBT based 3L-ANPC inverter. The cumulative energy loss for the Si IGBT based inverter is around 64.1 kWh, and in contrast, for the GaN-based inverter at 10 kHz and 300 kHz is 16.8 kWh and 63.9 kWh, respectively. At the switching frequency of 300 kHz, although the GaN HEMTs are switched 30 times more than Si IGBTs, the associated additional energy losses due to the increased switching frequency is 74% of the total energy losses of the Si IGBT based inverter. The average electricity price in Denmark for household consumers is 0.304 €/kWh [43]. Without considering thermal benefits of reduced converter losses, if the feed-in tariff is assumed to be same as the utility tariff, it can be concluded that the GaN HEMT based inverter at 10 kHz will bring additional €30.73 to the owner in comparison to the Si IGBT based inverter. At 300 kHz, the GaN HEMT based inverter will not bring significant operation income to the owner, whereas will provide reduction in initial system cost saving due to the reduction in cooling and output filtering requirements [20].

Conduction and switching loss breakdown of the Si and GaN based inverter phase leg are presented in Fig. 9. with respect to four different ambient temperatures and at maximum solar irradiance for the given ambient temperature profile. At 10 kHz switching frequency, the conduction losses are dominating the overall converter losses for the Si IGBTs. Meanwhile, the losses reduce with respect to the temperature increase due to the reduction in the input power and relatively small temperature dependence of conduction performance of Si IGBTs at low collector current levels as shown in Table II, despite the fact that switching losses increase according to ambient temperature. On the other hand, the switching losses of the GaN HEMT based inverter leg is negligible at 10 kHz and the total losses are dominated by the conduction losses. The switching losses increase as the switching frequency is moved from 10 kHz to 300 kHz in Fig. 9 (b) and (c), but the overall losses of the phase leg is close to Si IGBT based inverters, as it is shown in Fig. 9 (a).

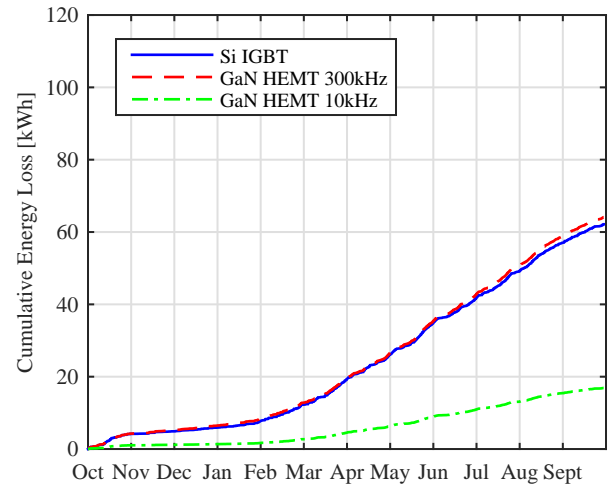
As the size of heat sink volume is inversely proportional to required thermal resistance $Z_{th(ch)}$ [20], [37], the heat sink volume of the GaN HEMT based inverter at 300 kHz will still be smaller than that in the case of the Si based inverter. Therefore, heat sink can still contribute to system level cost saving for the GaN based inverter at a very high switching frequency.

B. Thermal Stress Comparison

The applied modulation scheme in Fig. 2 provides low conduction losses with the penalty of uneven loss distribution in the 3L-ANPC phase leg at unity power factor operation. During positive half cycle of the output voltage, S_1 is subject



(a)



(b)

Fig. 8: Estimated annual power losses and cumulative energy loss of the ANPC inverter based on different technologies using the mission-profile analysis approach: (a) annual power losses and (b) cumulative energy losses.

to hard switching and also conducts during active state, while S_3 conducts during positive and zero states, and S_2 only conducts during zero states. Therefore, it is expected to see highest power losses across S_1 or S_3 switches depending on the device switching, conduction performance and inverter switching frequency. The loss distributions for upper devices in the 3L-ANPC - phase leg-A in Fig. 1 are presented in Fig. 10 for Si and GaN. In the Si-based inverter, due to the unity power factor operation, antiparallel diodes D_2 and D_3 only conduct during positive and negative zero states. Although S_3 has higher conduction losses than S_1 , S_1 has the highest losses in the inverter leg due to the switching loss contribution presented in Fig. 9 (a). On the other side, for the GaN based inverter at 10 kHz and 300 kHz in Fig. 10 (b) and (c), the loss distributions among S_1 and S_3 vary with respect to the

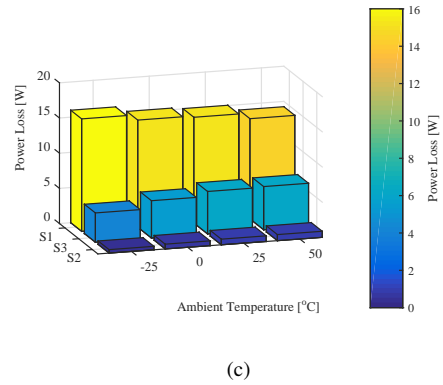
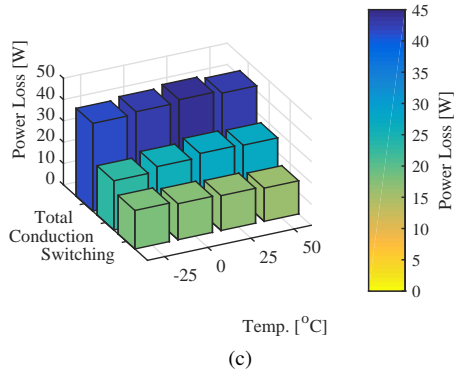
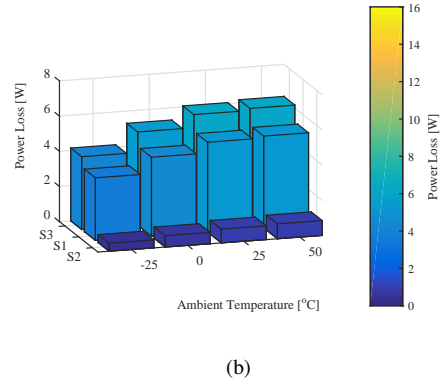
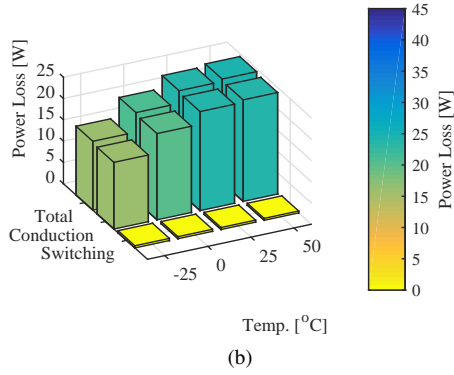
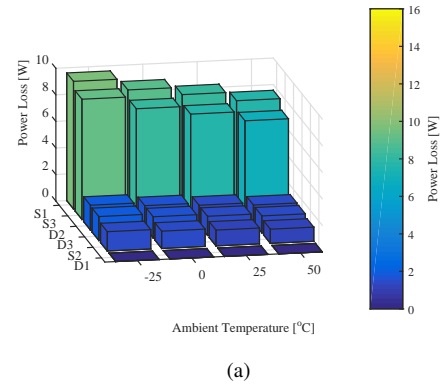
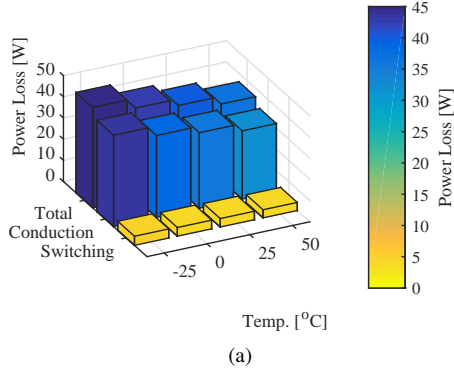


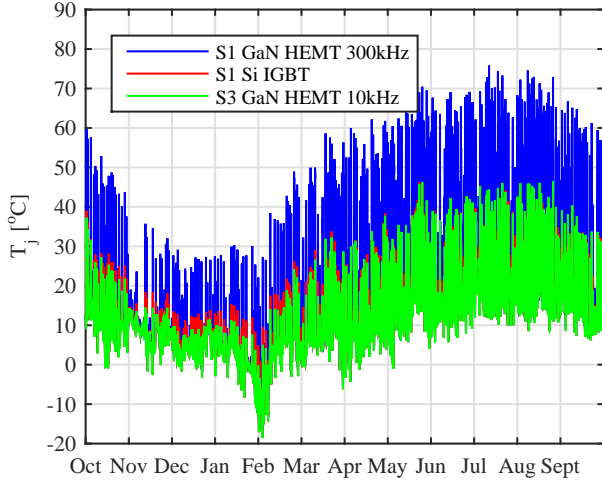
Fig. 9: Semiconductor total, conduction, and switching losses per phase leg of the ANPC inverter based on: (a) Si IGBT technology with a switching frequency of 10 kHz, (b) GaN technology with a switching frequency of 10 kHz, and (c) GaN technology with a switching frequency of 300 kHz, where different ambient temperatures with the maximum solar irradiance level are considered.

Fig. 10: Loss distribution of the ANPC inverter based on: (a) Si IGBT technology with a switching frequency of 10 kHz, (b) GaN technology with a switching frequency of 10 kHz, and (c) GaN technology with a switching frequency of 300 kHz, where different ambient temperatures with the maximum solar irradiance level are considered.

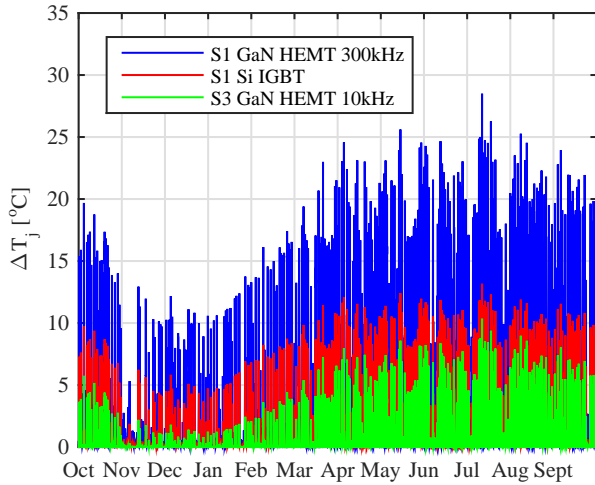
selected switching frequency. High switching performance of the GaN HEMTs shows the impact at 10 kHz by keeping power losses of S_1 less than S_3 . By increasing the switching frequency to 300 kHz, switching losses become significant in overall losses (Fig. 9 (c)), resulting in that S_1 has the highest power loss in the inverter leg.

As the devices with highest power losses and therefore the thermal stress in each configuration are identified, further thermal performance analysis can be conducted on these devices based on the annual mission profile. Mean junction

temperature (T_j) and junction temperature variation (ΔT_j) for devices with the highest thermal stress are presented in Fig. 12 (a) and (b), respectively. Mean junction temperature of S_1 in a Si IGBT based inverter is below 50 °C, while the mean junction temperature of S_1 in the GaN HEMT based inverter with 300 kHz switching frequency can go up to 75 °C during summer time. The mean junction temperature follows the ambient temperature trend throughout the year and can show significant variations based on the solar irradiance and ambient temperature. Regarding the junction temperature variations,



(a)



(b)

Fig. 11: Thermal loading profiles for the most stressed devices in 3L-ANPC inverter through a year: (a) mean junction temperature and (b) junction temperature variation.

S_1 in a GaN HEMT inverter with 300 kHz has the highest temperature variation across the junction of the device. S_3 in a GaN HEMT inverter at 10 kHz has a similar performance during warm months to that of S_1 in a Si IGBT inverter due to the increased conduction losses.

It can be seen from Fig. 12 that the long term mean junction temperature and junction temperature fluctuations are irregular profiles with varying frequencies and amplitudes. In order to make the results more meaningful, cycling counting methods can be applied to the mean junction temperature and junction temperature variation data. The number of cycles at each temperature level is dependent to mission profile, thermal and electrical models as it is explained in the previous sections. Rainflow is one of the cycle-counting methods to identify full and half cycles within irregular profiles, and is chosen in this study. It has been used in calculation of lifetime of

power modules based on device solder temperature profiles [44]. The histograms of mean junction temperature (T_j) and junction temperature variations (ΔT_j) are presented for the most stressed devices are presented in Fig. ?? (a) and (b), respectively. Replacing Si IGBTs with GaN HEMTs at 10 kHz switching frequency reduces the number of cycles at higher temperatures. On the other hand, the GaN HEMTs with 300 kHz switching frequency have increased T_j and ΔT_j at higher temperatures, which means that the device is subject to higher thermal stresses in comparison to other two options.

The Coffin-Manson model for conventional power modules indicates that number of failures in a power module is only dependent on the temperature cycles, cycle amplitude ΔT_j and mean junction temperature T_j [45]. Therefore, with adequate device packaging models for the GaN HEMTs and Si IGBTs, lifetime consumption of the power devices at different switching frequencies can be calculated and then an optimisation between reliability, efficiency and system volume can be achieved.

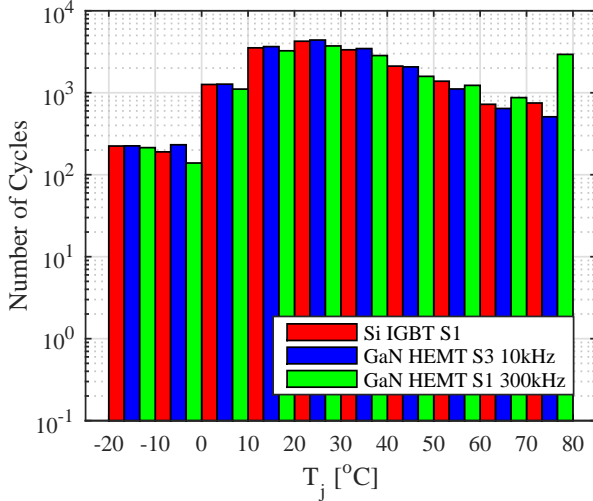
C. Thermal Interface Material Impact on GaN HEMT

As it is mentioned earlier, the thermally-conductive insulator (thermal interface material, TIM) with 4 °K/W thermal resistance has been placed between the thermal pad of the GaN HEMT and the heat sink. As the junction-to-case thermal resistance of GaN HEMTs is extremely low, the thermal resistance of TIM will increase the thermal stress across the GaN power devices. In order to illustrate this, the mean junction and junction temperature variation of S_3 in a GaN HEMT inverter at 10 kHz switching frequency with and without TIM are presented in Fig. 13. It is clear that the mean temperature can increase by 10 °C during warm days and the maximum junction temperature variation can increase from 5 to 10 °C. The histograms based on mean junction temperature and junction temperature variations in Fig. 13 are presented in Fig. 14 (a) and (b) respectively. The histogram results show that number of cycles for mean junction temperature and junction temperature variation is higher with TIM. Therefore, innovative cooling solutions are required for the GaN packages that provide excellent electrical isolation without compromising thermal performance of the devices.

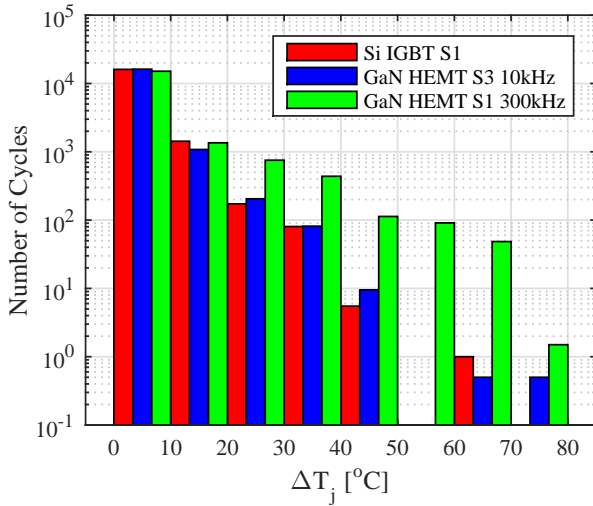
IV. EXPERIMENTAL RESULTS

The performance of 600 V Si IGBTs has been well studied in literature for different applications and some these results have been discussed in the introduction section of this paper. On the other hand, normally-off 650 V GaN HEMTs with low inductance package recently emerged for power electronic applications. Therefore, a GaN HEMT based single phase ANPC inverter demonstrator has been designed and built. The performance of GaN HEMT devices is experimentally evaluated and presented in this section.

The GaN HEMT based single phase ANPC inverter is presented in Fig. 15. The power cell is formed by four-layer PCB with 140 μm copper on each layer. The power cell consists of high frequency DC link capacitors, GaN HEMT



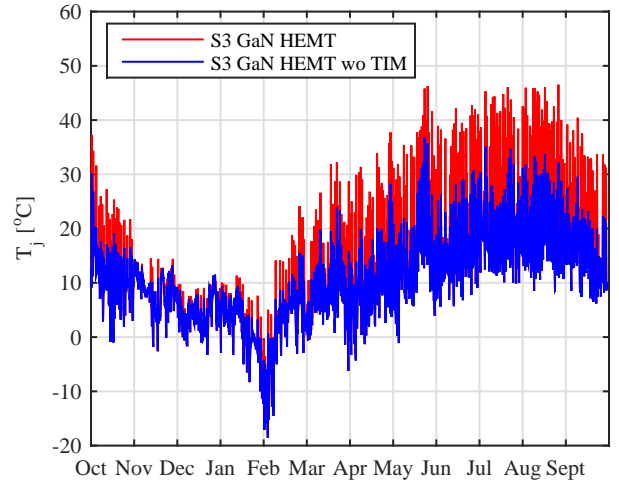
(a)



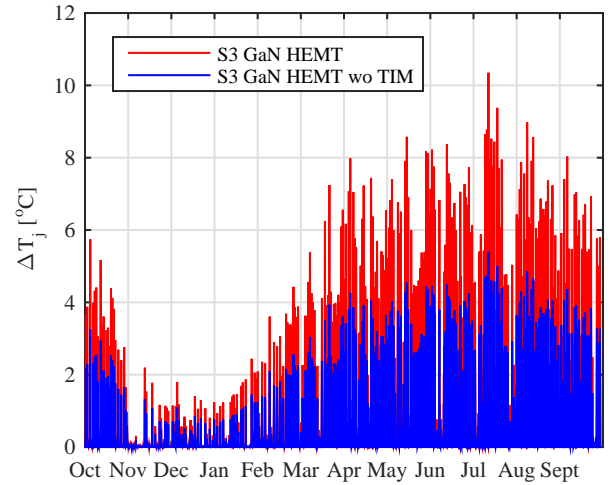
(b)

Fig. 12: Rainflow counting results for the thermal loading profiles shown in Fig. 11 under a yearly mission profile: (a) mean junction temperature and (b) cycle amplitude.

switches, gate drivers, signal and power isolation circuits for gate drivers and fibre optic receivers for gate signals. The $S_1 - S_3$ GaN devices are placed on top side of the PCB while $S_4 - S_6$ GaN devices are placed on bottom side of the PCB in symmetry to $S_1 - S_3$ for minimised commutation loop and high switching speed. The PCB is designed to have a modular system with the option to extend the demonstrator to three-phase by stacking PCBs vertically. Regarding cooling of power switches, two commercial heat sinks, which are joined by 4 screws with compression springs in order to apply equal contact pressure to the devices from top and bottom part of the PCB. The PCB has been presented without heat sinks in order to show device positions on the board.



(a)



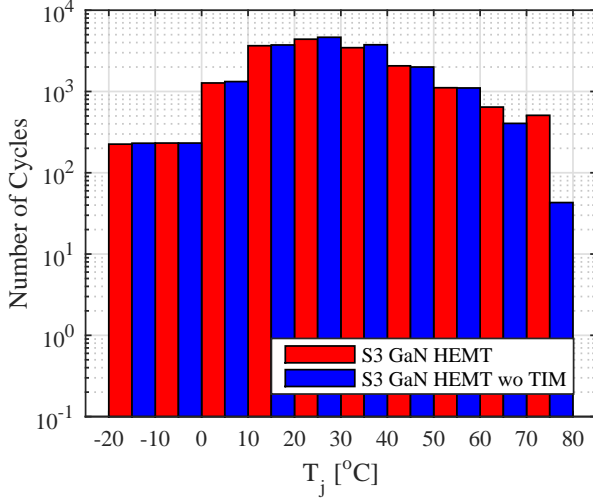
(b)

Fig. 13: Thermal loading of the S_3 GaN HEMT in the 3L-ANPC inverter with and without electrical insulation (TIM) material: (a) mean junction temperature and (b) junction temperature variation.

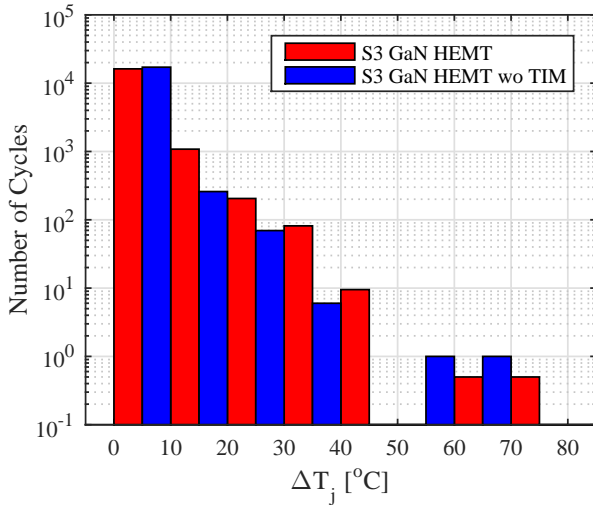
A. Switching Performance

The ANPC power cell is initially operated as a buck DC/DC converter in order to evaluate switching performance of GaN devices and designed power cell. For buck configuration, upper switches $S_1 - S_3$ are used where S_3 is completely on during the switching period and complementary gate signals are applied to S_1 and S_2 with 200 ns dead-time.

The switching waveforms at 40 kHz switching frequency with 400 V DC link voltage and 1 kW output power are presented in Fig. 16. In Fig. 16 (b), the output current commutates from S_2 to S_1 and S_1 is subject to hard-switching. The commutation from S_1 to reverse conduction of S_2 is presented in Fig. 16 (c). Drain-source voltage waveforms V_{DS1} and V_{DS2} prove high switching speed of GaN HEMTs with 13.2 ns rise and fall time of V_{DS2} and V_{DS1} respectively.



(a)



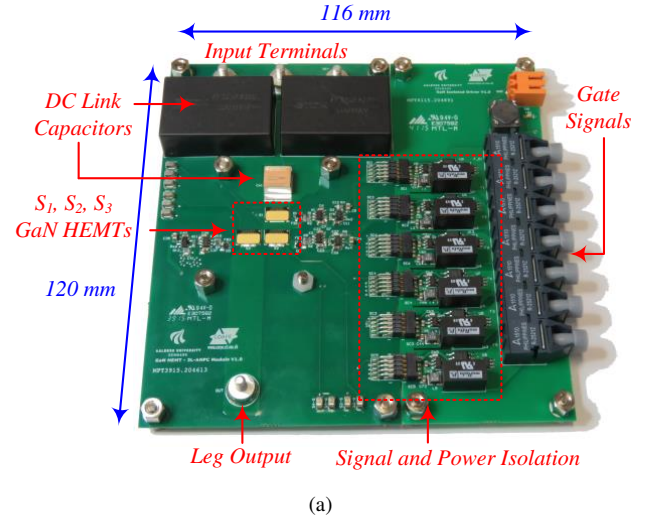
(b)

Fig. 14: Rainflow counting results of the thermal loading profile shown in Fig. 13 (for the S_3 GaN HEMT device) with and without electrical insulation material: mean junction temperature and (b) junction temperature variations.

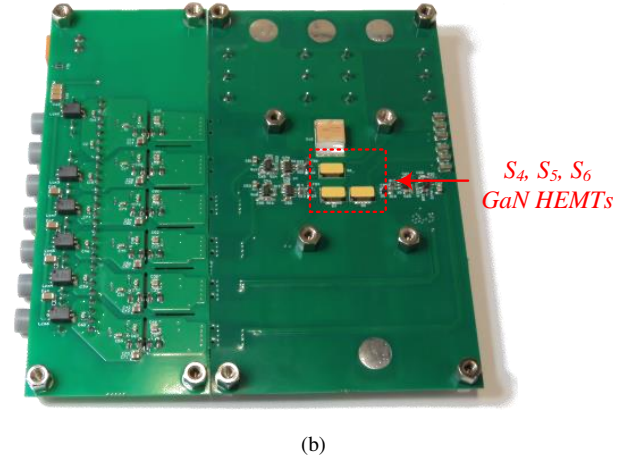
B. Inverter Performance

The single phase 3L-ANPC inverter prototype in Fig. 15 is tested with 700 V DC link, 10 kHz switching frequency to demonstrate performance of GaN based power cell without heat sink. The inverter test setup is presented in Fig. 17. The inverter is powered by a DC power supply with DC link decoupling capacitors. An RL load configuration is used for evaluation of performance under different load conditions. Efficiency and losses of power cell is measured by Yokogawa WT3000E precision power analyser with 0.01% power accuracy.

The experimental output current and voltage waveforms, and power cell efficiency with experimental and simulation results are presented in Fig. 18 (a) and (b), respectively. The experimental results support validity of high performance of



(a)



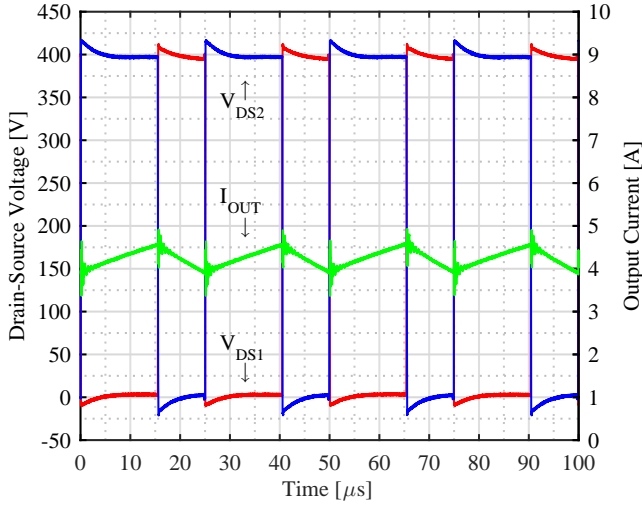
(b)

Fig. 15: Hardware of the GaN HEMT based single phase ANPC power cell: (a) top view and (b) bottom view.

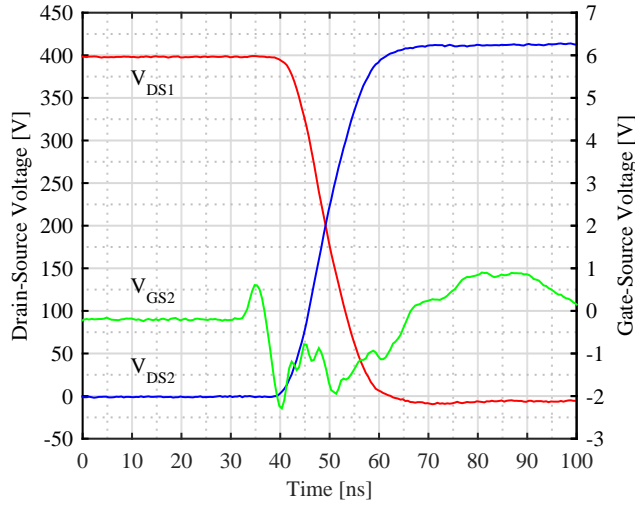
GaN HEMT devices in simulation and comparison with Si IGBTs. The efficiency comparison in Fig. 18 (b) validates the performance assumption of GaN HEMTs in the inverter operation mode.

V. CONCLUSION

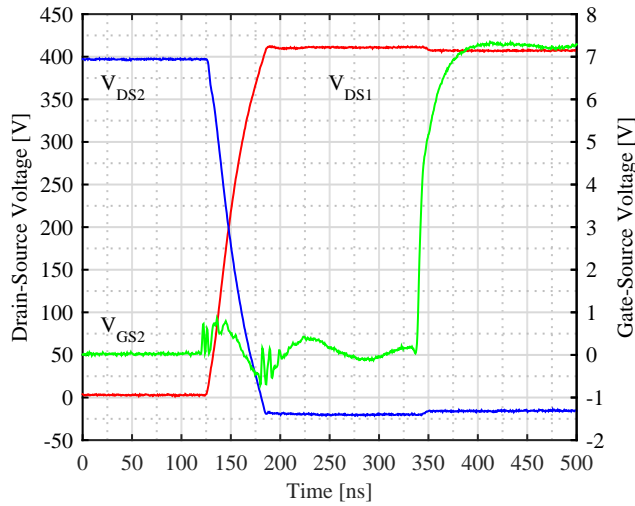
This paper has explored the challenging issues and the possibility of moving to new technologies namely GaN HEMTs in PV inverters, with special focus on the reliability and thermal performance. A comparison of Si IGBT against GaN HEMT with three different possibilities: 1) with TIM at 10 kHz, 2) without TIM at 10 kHz, and 3) with TIM at 300 kHz has been performed. Considering a long term mission profile, the results suggest higher reliability expectation for GaN HEMTs at low frequencies due to considerably lower power losses and thermal resistance between junction and heat sink, whereas TIM has contributed to significant additional thermal stress. Experimental results of single phase inverter prove high performance of GaN HEMT devices. The results in this paper are fundamental to confidently predict lifetime of



(a)



(b)



(c)

Fig. 16: Switching performance of the GaN HEMT in the 3L-ANPC inverter: (a) device voltage and output current, (b) hard commutation and (c) soft commutation waveforms with buck configuration.

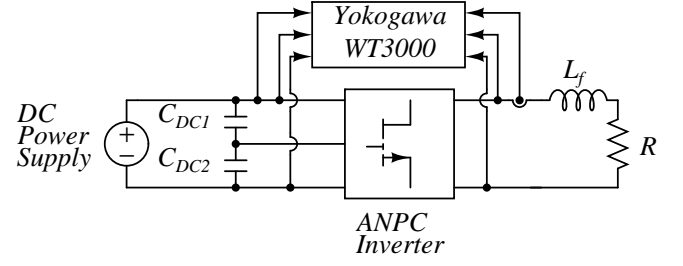
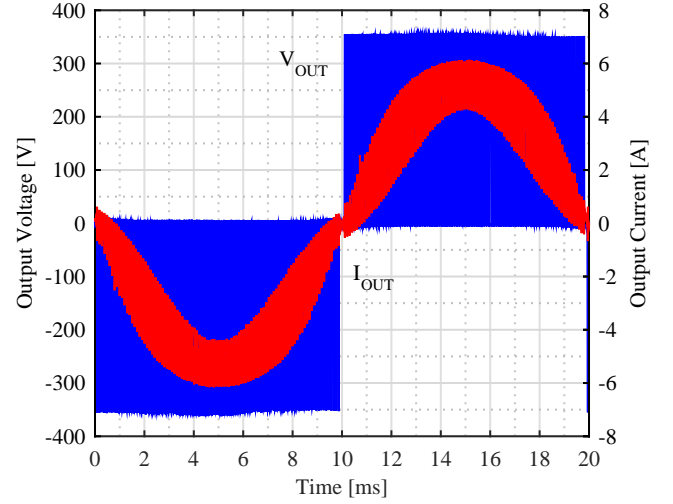
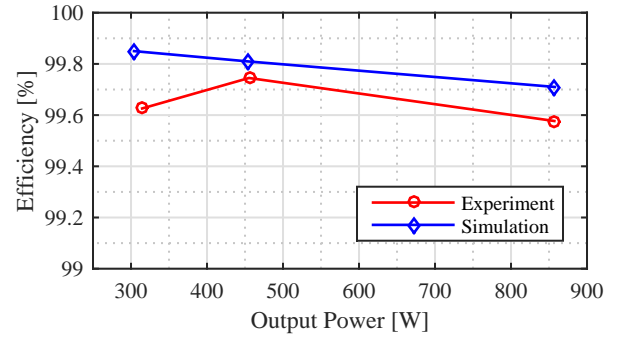


Fig. 17: Inverter test setup.



(a)



(b)

Fig. 18: (a) Experimental output voltage and current waveforms at 800 W output power and (b) efficiency of the 3L-ANPC power cell with experimental and simulation results.

novel GaN based PV inverters considering long term mission profiles.

ACKNOWLEDGEMENT

Authors would like to thank Geoff Haynes from GaN Systems for constructive discussions and providing detailed data about GaN HEMT devices.

REFERENCES

- [1] European Photovoltaic Industry Association, "Global Market Outlook For PV until 2018," 2014.

- [2] S. Kjaer, J. Pedersen, and F. Blaabjerg, "A Review of Single-Phase Grid-Connected Inverters for Photovoltaic Modules," *IEEE Transactions on Industry Applications*, vol. 41, no. 5, pp. 1292–1306, sep 2005.
- [3] J. Carrasco, L. Franquelo, J. Bialasiewicz, E. Galvan, R. PortilloGuisado, M. Prats, J. Leon, and N. Moreno-Alfonso, "Power-Electronic Systems for the Grid Integration of Renewable Energy Sources: A Survey," *IEEE Transactions on Industrial Electronics*, vol. 53, no. 4, pp. 1002–1016, jun 2006.
- [4] D. Meneses, F. Blaabjerg, O. Garcia, and J. a. Cobos, "Review and Comparison of Step-Up Transformerless Topologies for Photovoltaic AC-Module Application," *IEEE Transactions on Power Electronics*, vol. 28, no. 6, pp. 2649–2663, 2013.
- [5] T. Kerekes, R. Teodorescu, P. Rodriguez, G. Vazquez, and E. Aldabas, "A New High-Efficiency Single-Phase Transformerless PV Inverter Topology," *IEEE Transactions on Industrial Electronics*, vol. 58, no. 1, pp. 184–191, jan 2011.
- [6] E. Gubía, P. Sanchis, A. Ursúa, J. López, and L. Marroyo, "Ground currents in single-phase transformerless photovoltaic systems," *Progress in Photovoltaics: Research and Applications*, vol. 15, no. 7, pp. 629–650, nov 2007.
- [7] J. Millan, P. Godignon, X. Perpina, A. Perez-Tomas, and J. Rebollo, "A Survey of Wide Bandgap Power Semiconductor Devices," *IEEE Transactions on Power Electronics*, vol. 29, no. 5, pp. 2155–2163, may 2014.
- [8] C. Wilhelm, D. Kranzer, and B. Burger, "Development of a highly compact and efficient solar inverter with Silicon Carbide transistors," in *Integrated Power Electronics Systems (CIPS)*, 2010, 2010, pp. 1–6.
- [9] B. Burger and D. Kranzer, "Extreme high efficiency PV-power converters," in *Power Electronics and Applications, 2009. EPE '09.*, 2009, pp. 1–13.
- [10] D. Kranzer, C. Wilhelm, F. Reinert, and B. Burger, "Application of normally-off SiC-JFETs in photovoltaic inverters," in *Power Electronics and Applications, 2009. EPE '09.*, 2009, pp. 1–6.
- [11] D. Bergogne, D. Risaletto, F. Dubois, A. Hammoud, H. Morel, P. Bevilacqua, B. Allard, O. Berry, F. MeibodyTabar, S. Rael, R. Meuret, and S. Dhokkar, "Normally-On SiC JFETs in power converters: Gate driver and safe operation," *2010 6th International Conference on Integrated Power Electronics Systems*, pp. 1–6, 2010.
- [12] E. Gurpinar, D. De, A. Castellazzi, D. Barater, G. Buticchi, and G. Francheschini, "Performance analysis of SiC MOSFET based 3-level ANPC grid-connected inverter with novel modulation scheme," in *2014 IEEE 15th Workshop on Control and Modeling for Power Electronics (COMPEL)*. IEEE, jun 2014, pp. 1–7.
- [13] D. De, A. Castellazzi, A. Solomon, A. Trentin, M. Minami, and T. Hikiyara, "An all SiC MOSFET high performance PV converter cell," in *2013 15th European Conference on Power Electronics and Applications, EPE 2013*. IEEE, sep 2013, pp. 1–10.
- [14] D. Barater, C. Concari, G. Buticchi, E. Gurpinar, D. De, and A. Castellazzi, "Performance evaluation of a 3-level ANPC photovoltaic grid-connected inverter with 650V SiC devices and optimized PWM," in *2014 IEEE Energy Conversion Congress and Exposition (ECCE)*. IEEE, sep 2014, pp. 2233–2240.
- [15] A. Hensel, C. Wilhelm, and D. Kranzer, "Application of a new 600 V GaN transistor in power electronics for PV systems," in *2012 15th International Power Electronics and Motion Control Conference (EPE/PEMC)*. IEEE, sep 2012, pp. DS3d.4–1–DS3d.4–5.
- [16] T. Ueda, "Recent advances and future prospects on GaN-based power devices," in *2014 International Power Electronics Conference (IPEC-Hiroshima 2014 - ECCE ASIA)*. IEEE, may 2014, pp. 2075–2078.
- [17] T. Morita, S. Tamura, Y. Anda, M. Ishida, Y. Uemoto, T. Ueda, T. Tanaka, and D. Ueda, "99.3% Efficiency of three-phase inverter for motor drive using GaN-based Gate Injection Transistors," in *2011 Twenty-Sixth Annual IEEE Applied Power Electronics Conference and Exposition (APEC)*. IEEE, mar 2011, pp. 481–484.
- [18] A. Tuysuz, R. Bosshard, and J. W. Kolar, "Performance comparison of a GaN GIT and a Si IGBT for high-speed drive applications," in *2014 International Power Electronics Conference (IPEC-Hiroshima 2014 - ECCE ASIA)*. IEEE, may 2014, pp. 1904–1911.
- [19] E. Gurpinar and A. Castellazzi, "SiC and GaN based BSNPC inverter for photovoltaic systems," in *2015 17th European Conference on Power Electronics and Applications (EPE'15 ECCE-Europe)*. IEEE, sep 2015, pp. 1–10.
- [20] —, "Single-phase t-type inverter performance benchmark using si ighs, sic mosfets and gan hems," *IEEE Transactions on Power Electronics*, vol. PP, no. 99, pp. 1–1, 2015.
- [21] X. Huang, Z. Liu, Q. Li, and F. C. Lee, "Evaluation and Application of 600 V GaN HEMT in Cascode Structure," *IEEE Transactions on Power Electronics*, vol. 29, no. 5, pp. 2453–2461, may 2014.
- [22] T. Ishibashi, M. Okamoto, E. Hiraki, T. Tanaka, T. Hashizume, D. Kikuta, and T. Kachi, "Experimental Validation of Normally-On GaN HEMT and Its Gate Drive Circuit," *IEEE Transactions on Industry Applications*, vol. 51, no. 3, pp. 2415–2422, may 2015.
- [23] Y. Yang, P. Enjeti, F. Blaabjerg, and H. Wang, "Wide-Scale Adoption of Photovoltaic Energy: Grid Code Modifications Are Explored in the Distribution Grid," *IEEE Industry Applications Magazine*, vol. 21, no. 5, pp. 21–31, 2015.
- [24] E. Koutroulis and F. Blaabjerg, "Design Optimization of Transformerless Grid-Connected PV Inverters Including Reliability," *IEEE Transactions on Power Electronics*, vol. 28, no. 1, pp. 325–335, 2013.
- [25] Y. Yang, H. Wang, F. Blaabjerg, and K. Ma, "Mission profile based multi-disciplinary analysis of power modules in single-phase transformerless photovoltaic inverters," in *2013 15th European Conference on Power Electronics and Applications (EPE)*. IEEE, sep 2013, pp. 1–10.
- [26] A. Anurag, Y. Yang, and F. Blaabjerg, "Thermal Performance and Reliability Analysis of Single-Phase PV Inverters with Reactive Power Injection Outside Feed-In Operating Hours," *IEEE Journal of Emerging and Selected Topics in Power Electronics*, vol. 6777, no. 99, pp. 1–1, 2015.
- [27] N.-c. Sintamarean, F. Blaabjerg, H. Wang, F. Iannuzzo, and P. D. P. Rikken, "Reliability Oriented Design Tool For the New Generation of Grid Connected PV-Inverters," *IEEE Transactions on Power Electronics*, vol. 30, no. 5, pp. 2635–2644, 2015.
- [28] S. Kouro, J. I. Leon, D. Vinnikov, and L. G. Franquelo, "Grid-Connected Photovoltaic Systems: An Overview of Recent Research and Emerging PV Converter Technology," *Industrial Electronics Magazine, IEEE*, vol. 9, no. 1, pp. 47–61, 2015.
- [29] T. Bruckner, S. Bernet, and H. Guldner, "The Active NPC Converter and Its Loss-Balancing Control," *IEEE Transactions on Industrial Electronics*, vol. 52, no. 3, pp. 855–868, jun 2005.
- [30] A. Nabae, I. Takahashi, and H. Akagi, "A New Neutral-Point-Clamped PWM Inverter," *IEEE Transactions on Industry Applications*, vol. IA-17, no. 5, pp. 518–523, sep 1981.
- [31] J. Rodriguez, S. Bernet, B. Wu, J. O. Pontt, and S. Kouro, "Multilevel Voltage-Source-Converter Topologies for Industrial Medium-Voltage Drives," *IEEE Transactions on Industrial Electronics*, vol. 54, no. 6, pp. 2930–2945, dec 2007.
- [32] T. Bruckner, S. Bernet, and P. K. Steimer, "Feedforward Loss Control of Three-Level Active NPC Converters," *IEEE Transactions on Industry Applications*, vol. 43, no. 6, pp. 1588–1596, 2007.
- [33] P. Barbosa, P. Steimer, J. Steinke, M. Winkelkemper, and N. Celanovic, "Active-neutral-point-clamped (ANPC) multilevel converter technology," in *2005 European Conference on Power Electronics and Applications*. IEEE, 2005, pp. 10 pp.–P.10.
- [34] D. Florica, E. Florica, and M. Dumitrescu, "Natural doubling of the apparent switching frequency using three-level ANPC converter," in *2008 International School on Nonsinusoidal Currents and Compensation*, vol. 2. IEEE, jun 2008, pp. 1–6.
- [35] Y. Jiao, S. Lu, and F. Lee, "Switching Performance Optimization of a High Power High Frequency 3-level Active Neutral Point Clamped Phase Leg Building Block," *IEEE Transactions on Power Electronics*, no. c, pp. 1–1, 2013.
- [36] J. Mookken, B. Agrawal, and J. Liu, "Efficient and Compact 50kW Gen2 SiC Device Based PV String Inverter," in *PCIM Europe 2014; International Exhibition and Conference for Power Electronics, Intelligent Motion, Renewable Energy and Energy Management; Proceedings of*, may 2014, pp. 1–7.
- [37] J.-i. Itoh and T. Araki, "Volume evaluation of a PWM inverter with wide band-gap devices for motor drive system," in *2013 IEEE ECCE Asia Downunder*. IEEE, jun 2013, pp. 372–378.
- [38] P. Anthony and N. McNeill, "The efficient deployment of silicon superjunction MOSFETs as synchronous rectifiers," in *7th IET International Conference on Power Electronics, Machines and Drives (PEMD 2014)*. Institution of Engineering and Technology, 2014, pp. 0185–0185.
- [39] M. Conrad and R. W. DeDoncker, "Avoiding reverse recovery effects in super junction MOSFET based half-bridges," in *2015 IEEE 6th International Symposium on Power Electronics for Distributed Generation Systems (PEDG)*. IEEE, jun 2015, pp. 1–5.
- [40] GaN Systems, "GaNPX Packaging." [Online]. Available: http://www.gansystems.com/ganpx_packaging_new.php
- [41] "Bergquist Sil-Pad 2000." [Online]. Available: http://www.bergquistcompany.com/thermal_materials/sil_pad/sil-pad-2000_properties.htm

- [42] "Bergquist Sil-Pad 2000, 2015-54 TO-220." [Online]. Available: http://www.bergquistcompany.com/pdfs/dataSheets/PDS_SP_2000_0410.pdf
- [43] "Energy price statistics - Statistics Explained." [Online]. Available: http://ec.europa.eu/eurostat/statistics-explained/index.php/Energy_price_statistics
- [44] M. Musallam and C. M. Johnson, "An Efficient Implementation of the Rainflow Counting Algorithm for Life Consumption Estimation," *IEEE Transactions on Reliability*, vol. 61, no. 4, pp. 978–986, dec 2012.
- [45] Y. Yang, H. Wang, and F. Blaabjerg, "Improved reliability of single-phase PV inverters by limiting the maximum feed-in power," in *2014 IEEE Energy Conversion Congress and Exposition (ECCE)*. IEEE, sep 2014, pp. 128–135.



Emre Gurpinar (S'11) received the Bachelor's of Science degree in electrical engineering from Istanbul Technical University, Istanbul, Turkey, in 2009 and the Master's of Science degree in power electronics, machines and drives from the University of Manchester, Manchester, U.K. in 2010. Since 2013, he has been working toward the Ph.D. degree at the University of Nottingham, U.K. He is currently working on his Ph.D. thesis based on wide-bandgap semiconductor based renewable power converters.

He was a visiting Ph.D. student with the Department of Energy Technology, Aalborg University, Denmark, between August 2015 and October 2015.

He was an R&D Power Electronics Engineer with General Electric, U.K. His research interest include wide-bandgap power devices, high-frequency converters, renewable power systems, and hybrid multilevel inverters.

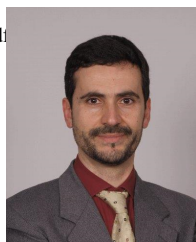


Yongheng Yang (S'11-M'15) received the B.Eng. degree from Northwestern Polytechnical University, Xian, China, in 2009, and the Ph.D. degree from Aalborg University, Aalborg, Denmark, in 2014.

He was a Post-Graduate with Southeast University, Nanjing, China, from 2009 to 2011. In 2013, he was a Visiting Scholar with the Department of Electrical and Computer Engineering, Texas A&M University, College Station, USA. Since 2014, he has been with the Department of Energy Technology, Aalborg University, where he is currently an

Assistant Professor. His research interests are focused on grid integration of renewable energy systems, power converter design, analysis and control, harmonics identification and mitigation, and reliability in power electronics.

Dr. Yang is a Member of the IEEE Power Electronics Society Students and Young Professionals Committee, where he is responsible for the webinar series. He serves as a Guest Associate Editor of the IEEE JOURNAL OF EMERGING AND SELECTED TOPICS IN POWER ELECTRONICS special issue on Power Electronics for Energy Efficient Buildings. Dr. Yang has also been invited as a Guest Editor of Applied Sciences special issue on Advancing Grid-Connected Renewable Generation Systems. He is an active reviewer for relevant top-tier journals.



Francesco Iannuzzo (M'04-SM'12) received the M.Sc. degree in Electronic Engineering and the Ph.D. degree in Electronic and Information Engineering from the University of Naples, Italy, in 1997 and 2001, respectively. He is primarily specialized in power device modelling. From 2000 to 2006, he has been a Researcher with the University of Cassino, Italy, where he became Aggregate Professor in 2006 and he is currently Associate Professor since 2012. In 2014 he got a contract as professor in Reliable Power Electronics at the Aalborg University, Denmark, where he is also part of CORPE (Center Of Reliable Power Electronics, <http://www.corpe.et.aau.dk>). He is author or co-author of more than 100 publications on journals and international conferences, and one patent on an innovative inverter topology for very compact, galvanic-isolated auxiliary power supply for heavy train applications. His research interests are in the field of reliability of power devices, including cosmic rays, power device failure modelling and testing of power modules up to MW-scale under extreme conditions, like overvoltage, overcurrent, overtemperature and short circuit.

Prof. Iannuzzo was the Technical Programme Committee co-Chair in two editions of ESREF, the European Symposium on RELiability and Failure analysis. He is a senior member of the IEEE (Reliability Society, Electron Device Society, Industrial Electronic Society and Industry Application Society) and of AEIT (Italian Electric, Electronic and Telecommunication Association). He permanently serves as expert and peer reviewer for several conferences and journals in the field, like: APEC, ECCE, EPE, ESREF, IECON, Elsevier Microelectronics Reliability, IEEE Transactions on Industrial Electronics, Transactions on Industrial Informatics and Transactions on Power Electronics.



Alberto Castellazzi received the Laurea degree in physics from the University of Milan, Milan, Italy, in 1998 and the Ph.D. degree in electrical engineering from the Munich University of Technology, Munich, Germany, in 2004. He is an Associate Professor of power electronics with The University of Nottingham, Nottingham, U.K. He has been active in power electronics research and development for over 15 years and has had extensive collaborations with major European and international industrial research laboratories and groups on publicly and privately

funded research projects. He has authored or coauthored over 130 papers published in peer reviewed specialist journals and conference proceedings, for which he also regularly acts as a reviewer. His research interests include characterization, modelling, application, packaging and cooling of power devices. He is a member of the Technical Programme Committee of the ISPSD, ESTC and ECCE-Asia.



Frede Blaabjerg (S'86-M'88-SM'97-F'03) was with ABB-Scandia, Randers, Denmark, from 1987 to 1988. From 1988 to 1992, he was a Ph.D. Student with Aalborg University, Aalborg, Denmark. He became an Assistant Professor in 1992, Associate Professor in 1996, and Full Professor of power electronics and drives in 1998. His current research interests include power electronics and its applications such as in wind turbines, PV systems, reliability, harmonics and adjustable speed drives.

He has received 17 IEEE Prize Paper Awards, the IEEE PELS Distinguished Service Award in 2009, the EPE-PEMC Council Award in 2010, the IEEE William E. Newell Power Electronics Award 2014 and the Villum Kann Rasmussen Research Award 2014. He was an Editor-in-Chief of the IEEE TRANSACTIONS ON POWER ELECTRONICS from 2006 to 2012. He is nominated in 2014 and 2015 by Thomson Reuters to be between the most 250 cited researchers in Engineering in the world.